



Effects of Fiber Architectures on the Impact Resistance of Composite Laminates Under Low-Velocity Impact

Tianya Bian¹ · Qihui Lyu² · Xiaobin Fan¹ · Xiaomei Zhang¹ · Xiang Li¹ · Zaoyang Guo²

Received: 13 September 2021 / Accepted: 4 January 2022 / Published online: 23 January 2022
© The Author(s), under exclusive licence to Springer Nature B.V. 2022

Abstract

This present work focuses on evaluating the impact resistance of five marine superstructure laminated structures according to the engineering application requirements, which provide insights into the impact failure behaviors of marine composite laminates and are expected to aid material selection for marine superstructures. Evaluations were performed at different loads (6.7 J/mm, 8.7 J/mm, and 10.7 J/mm) using drop-weight impact and compression after impact tests to assess the resistances of fiber-architecture laminates to low-velocity impacts: carbon fiber, glass fiber, polyethylene (PE) fiber, carbon/PE hybrid, and carbon/glass hybrid laminates. The responses and damages of all laminates were then examined through force–time curves, force–displacement curves, visual damage inspection, ultrasonic C-scans, micrographs, and compression strength tests. The experimental results reveal that the hybrid fiber laminates inherit the characteristics of single-type laminates, resulting in positive hybrid synergistic effects. The carbon and PE fiber mix enhances the ductility and impact energy absorption of the fibers, while the hybrid carbon and glass fiber mix improves fiber toughness, thereby exhibiting higher impact resistance and damage tolerance.

Keywords Low-velocity impact behavior · Hybrid composite · Compression after impact · Damage tolerance · Damaged area

1 Introduction

Fiber-reinforced composite materials have high specific stiffness and strength, good corrosion resistance, and capacity to withstand fatigue; hence, they are widely used in marine applications, mainly for the construction of fast ferries, naval and coast guard patrol boats,

Tianya Bian and Qihui Lyu these authors contributed equally to this work.

✉ Qihui Lyu
m13019778011@163.com

✉ Zaoyang Guo
z-guo@foxmail.com

¹ Luoyang Ship Material Research Institute, Luoyang 471023, Henan, China

² School of Science, Harbin Institute of Technology, Shenzhen 518055, Guangdong, China

fishing boats, workboats, and offshore oil and gas installations [1]. However, composite structures are highly susceptible to impact events in actual marine environments, especially low-velocity impact (LVI) with solid objects, such as collisions with floating objects, other ships, docks, and production processes (e.g., tool drops), which drastically reduce their residual strengths [2–4]. Moreover, invisible cracks are formed inside the materials and extend sharply once concentrated stresses are applied, leading to eventual failure of the composite structures [5]. In recent times, considerable efforts have been made to investigate the impact resistances and damage tolerances of composite structures, and it is widely accepted that the mechanical properties required of composite materials in the marine industry can be achieved through different material combinations [6]. Therefore, it is necessary to study the damage modes and failure mechanisms of composite materials under impact and post-impact compression loads as well as explore materials that are highly resistant to damage in marine applications.

The most direct method to evaluate the impact resistance of a composite material or structure is to conduct LVI experiments and compression after impact (CAI) tests. It is noted that the duration of a typical LVI event is very small, usually between 1 and 10 ms, which makes it difficult to observe the initiation and evolution of the damage [7]. The impact resistance of the material can be obtained through the LVI test, that is, impact force, deflection, impact velocity and energy dissipation. And the CAI test is considered critical for the evaluation of the design process of the composite structure, which enables the assessment of reduction in strength of composite materials due to impact by means of uniform compression tests [8]. Researchers generally use nondestructive testing techniques, such as ultrasonic C-scan, X-ray computed tomography, and infrared thermal imaging, to determine the damage and better study the failure characteristics of composite laminates under impact loads [9]. Among them, the ultrasonic C-scan has been proved to be an efficient tool for detecting and quantifying delamination damage. X-ray computed tomography is used to evaluate the level of internal damage due to impact loading, after scanning, the raw data was used to reconstruct the 3D volume. And infrared thermal imaging can identify defects in the material by capturing and collecting the local heating process of the material. Further, infrared thermography is also employed to record a video during the impact event. Acoustic emission techniques and infrared thermography are two promising nondestructive online inspection methods for low-velocity impact events [10].

Hybridization of fiber-reinforced composites is expected to benefit from the advantages of the material properties of individual components. It is well known that carbon fibers have excellent mechanical properties but low impact resistance owing to their rigidity and fragility [11]. Therefore, carbon-fiber fabric is often used with fabrics made of other fibers to improve impact resistance [12, 13]. Chen et al. [14] studied the effects of carbon/glass/basalt hybrid fibers and fabric on the LVI resistance of fiber-reinforced plastic composites. It can be observed that the specimens hybridized with ductile fiber improved the impact resistance compared to non-hybrid CFRP laminate. Zhang et al. [15] evaluated the LVI properties of composite laminates with different mixing ratios of carbon and glass fiber warp-knitted fabric layers. The results indicated that the hybrid structure exhibited a positive hybrid effect in peak force and the absorbed energy, and the failure mechanism was significantly affected by the hybrid ratio and intralayer structure. Cheon et al. [16] used three different fiber-reinforced polymer composite materials to study the puncture resistance and blade penetration mechanisms of each type of reinforced plastic. The results showed that carbon/aramid composites had better stab resistance performances than the CFRP. And the hybridization provided a significant improvement in the damaged area and fiber breakage reduction of the CFRP. Hung et al.

[17] experimentally studied the LVI responses of hybrid carbon/glass fiber-reinforced polymer composites. They found that hybrid composite materials with carbon-fiber surface layers help minimize the risk of damage, whereas samples with glass-fiber surface layer and carbon-fiber core were seriously damaged. Liu et al. [18] compared the performances of hybrid UD /woven carbon-fiber-reinforced and pure UD carbon-fiber-reinforced composite laminates and showed that using woven piles on the top and bottom layers reduces the degree of damage in the event of an impact. Zhao et al. [19] studied the impact resistance of different composite plates to metallic projectiles. They observed that laminates stacked by angled unidirectional tapes contained impacts at higher velocities than other panels, while the energy absorption capacity of plain-woven and braided composite panels was comparable. Jakubczak et al. [20] researched the LVI properties of carbon-fiber-reinforced polymer, aluminum-carbon-reinforced aluminum, and titanium-carbon hybrid laminates and demonstrated that the impact resistance of the titanium-layer-based laminate was the best. Zhao et al. [21] conducted numerical simulations through high-speed impact tests combined with a multi-scale modeling framework to study the impact failure behavior of T700/3266 triaxial braided composite panels. They found that the braided structure showed good crack propagation resistance and interface delamination resistance, indicating that the material had excellent damage tolerance.

In addition to carbon fibers, other types of fiber-reinforced composite laminates have also been extensively studied by researchers. Aktaş et al. [22] conducted LVI tests on glass/epoxy composite laminate and it was observed that delamination and matrix cracking occurred at lower impact energies, while fiber damage occurred at higher impact energies. Evci et al. [23] evaluated unidirectional E-glass, woven E-glass, and woven aramid composite samples under LVI tests. The experimental results showed that woven composite materials had better damage resistance than unidirectional composite materials. Krollmann et al. [24] presented the impact behaviors of a specific hybrid matrix (HyMa) composite laminate under LVI tests, and the results showed that using the hybrid matrix (HyMa) laminates increased energy absorption by 21% with dramatic improvements in the impact resistance. Sanchez et al. [25] compared the CAI strengths of woven fabric and quasi-isotropic UD laminates to show that woven fabrics had higher CAI strengths owing to the increase in their interlaminar fracture toughness. Milad et al. [26] used acoustic emissions to characterize damages to non-crimp fabric (NCF), 2D plain-woven (2D-PW), and 3D orthogonal plain-woven (ORT-PW) carbon/epoxy laminates under impact loads. The results showed that ORT-PW laminates had the best performances for all architectures. Kapil et al. [27] explored the fabrication and investigation of the flexural strength of the hybrid FRPs material. The research showed that the accumulative Kevlar-glass combination offered higher resistance to bending than that of other combinations of natural and synthetic fibers.

Through the above research content, it can be found that the research on the impact of fiber-reinforced composite materials has been concerned by many scholars, but relatively few researches on the impact of marine superstructure materials have been published, which may be caused by military sensitivity or commercial nature. This article focuses on the needs of marine engineering applications and evaluates the impact resistance of five common marine superstructure laminated structures under the low-velocity impact, including three types of single fiber and two types of mixed fiber laminates. In addition to using the force–time and energy–time curves, the experimental results of the LVI test were studied by the CAI test and ultrasonic C-scan to evaluate the damage resistance and tolerance of each laminate for the selection of marine laminated materials.

Table 1 Physical properties of reinforcement and matrix

Reinforcement				Matrix	
Fiber	T300 Carbon fiber	E-Glass fiber	Polyethylene	Resin	430LV
Surface density	325 g/m ²	400 g/m ²	160 g/m ²	Density	1.14 g/cm ³
Yarn warp	T300-3 K	ELT400	T90-unidirectional	Viscosity	240 mPa·s
Tensile strength	3530 MPa	3100 MPa	2600 MPa		
Tensile modulus	230 GPa	86 GPa	77 GPa		

2 Experimental Procedures

2.1 Composite Materials

All the composite laminates used in this study were provided by Luoyang Ship Material Research Institute in China. The composite laminates considered herein were composed of T300 carbon fibers, E-glass fibers, and polyethylene (PE) fibers, and the three kinds of fibers are manufactured by Shanghai Jinhao fiber composite material Co., Ltd. in China. And the physical properties of laminates reinforcement and matrix are presented in Table 1. The carbon-fiber cloth used was a unidirectional belt of thickness 0.4 mm, while the glass and PE fiber cloths were plain-weave fabrics of thicknesses 0.35 mm and 0.33 mm, respectively. In the cloth layer, the warps were along the fiber direction and wefts were used to weave the fibers together through the string. And the laying process adopted was 0°/90° orthogonal laying. In addition, the matrices of all the laminates were made of 430LV, where the volume fraction of the resin was about 50%, the vacuum-assisted forming process was used, and post-curing treatment was carried out according to that for the resin matrix used to prepare the test specimens.

Table 2 lists the fiber compositions, stacking sequences, ply, and sizes of the five composite laminates, namely three single-type and two-hybrid laminates. The single-fiber laminates are carbon-fiber, glass-fiber, and PE laminates, and the hybrid laminates include those composed of carbon/PE fibers (C/P) and carbon/glass fibers (C/G). The five laminates used in this study are henceforth referred to as CF, GF, PE, C/P, and C/G.

2.2 LVI Setup

The impact tests for the composite laminates were conducted using the Wance Impact Testing Machine according to the standard ASTM D7136 “Standard test method for

Table 2 Laminates and their details

Laminate	Description	Stacking sequence	Number of fabric plies	Dimension (mm)
CF	Carbon fiber composite laminate	[(0/90) ₃] ₀ S	13	150×100×5.2
GF	Glass fiber composite laminate	[0/90] ₇	14	150×100×4.9
PE	PE fiber composite laminate	[(0/90) ₄] ₀ S	17	150×100×5.61
C/P	Alternate layering of CF and PE	[(0 _C /90 _{PE}) ₇ -0 _C] _S	15	150×100×5.51
C/G	Alternate layering of CF and GF	[(0 _C /90 _G) ₆ -0 _C] _S	13	150×100×4.9

measuring the damage resistance of a fiber-reinforced polymer matrix composite to a drop-weight impact event” [28]. As shown in Fig. 1, the specimens are clamped to an impact support fixture designed as per the ASTM standard, having a length of 125 ± 1 mm and a width of 75 ± 1 mm. And guiding pins shall be located such that the specimen shall be centrally positioned over the cut-out. Four clamps shall be used to restrain the specimen during impact. The smooth hemispherical impactor used in the test had a total mass of 5.5 ± 0.25 kg and a diameter of 16 ± 0.1 mm. The impactor acted on the center of the sample at a certain loading speed according to the set impact energy.

The measurement results show differences in the thicknesses of the five types of laminates. Therefore, when performing impact tests with the same absolute impact energy per unit thickness of the material, there may be false conclusions because thicker laminates have advantages over thinner laminates. To avoid such deviations, we referred to the

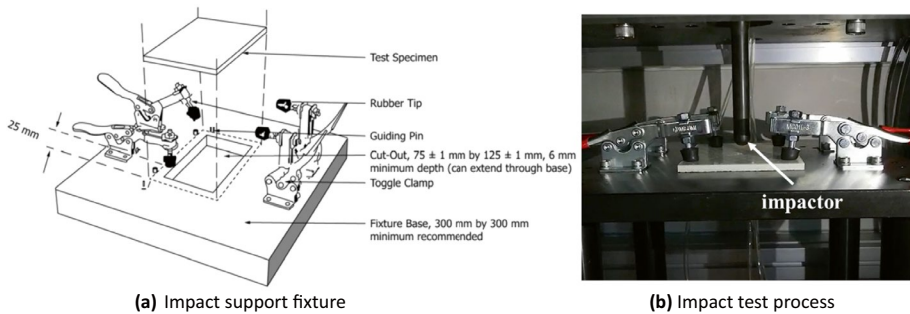
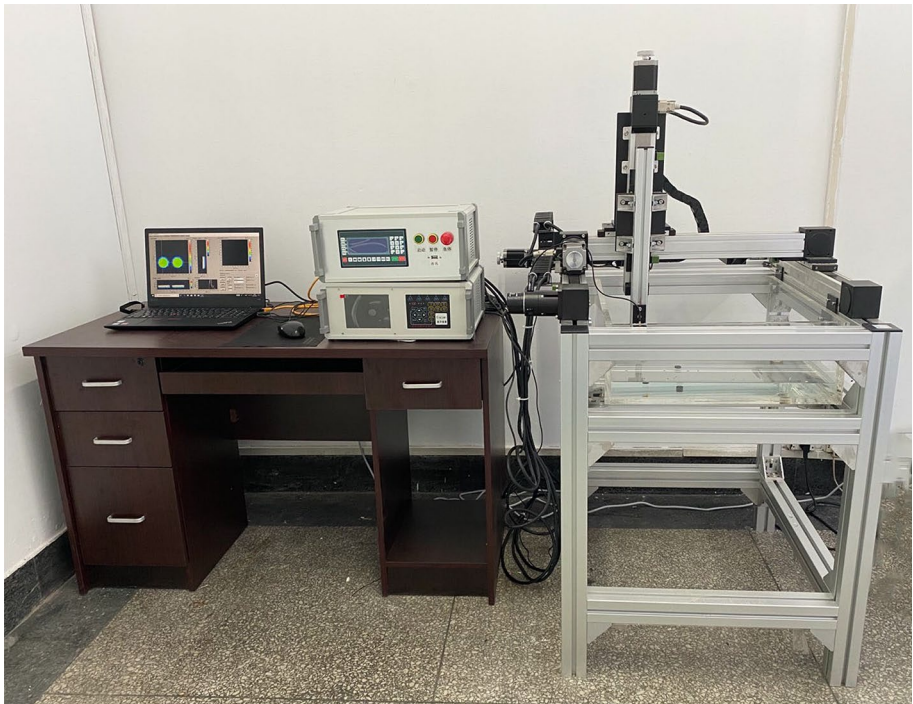


Fig. 1 Impact test platform

Table 3 Low-velocity impact test arrangements

Laminate	Measured laminate thickness (mm)	Normalized impact load 1:IE_1 (J/mm)	Normalized impact load 2:IE_2 (J/mm)	Normalized impact load 3:IE_3 (J/mm)
CF	5.3	6.7	8.7	10.7
GF	4.8	6.7	8.7	10.7
PE	5.6	6.7	8.7	10.7
C/P	5.6	6.7	8.7	10.7
C/G	5	6.7	8.7	10.7

ASTMD7136/D7136M-15 standards and adopted normalized impacts for the laminates based on their thicknesses [28]. A total of three normalized impact loads (6.7 J/mm, 8.7 J/mm, and 10.7 J/mm) were applied each to the five laminated plates, and these three values are correspondingly denoted as IE_1, IE_2, and IE_3. For each type of laminates, five identical plates were selected for the impact test to ensure the reliability and accuracy of the test. The impact force, deflection, impact velocity and energy dissipation were recorded using a digital data acquisition module, which was a NI USB-6531 data acquisition system with TestPilot_DIT software. Tables 2 and 3 also detail the stacking sequence, dimension and normalized impacts for all the laminates.

**Fig. 2** BSN-C1285 C-scan system

2.3 Determination of Impact Damage

For inspection of the impact samples, external evaluations were first performed, i.e., the damage degrees of the top and bottom were evaluated. Then, ultrasonic C-scan nondestructive testing was used to determine the damaged area. Owing to the scattering of ultrasonic waves, subsequent ultrasonic testing does not show the exact depth of delamination but can provide projection, such that the maximum area of delamination damage is the damaged area. As shown in Fig. 2, the water-immersion ultrasonic automatic imaging detection system BSN-C1285 was used to scan the impacted specimens, with a transmitter and a receiver transducer each of frequency 5 MHz. The color threshold and measurement function of ImageJ was used to analyze the C-scan images to determine the projected damaged areas of the specimens.

2.4 Post-impact Performance

CAI tests were performed on the specimens to evaluate their residual compressive strengths. Compression tests were performed on the 6.7, 8.7, and 10.7 J/mm impact specimens according to ASTM D7137 “Standard test method for compressive residual strength

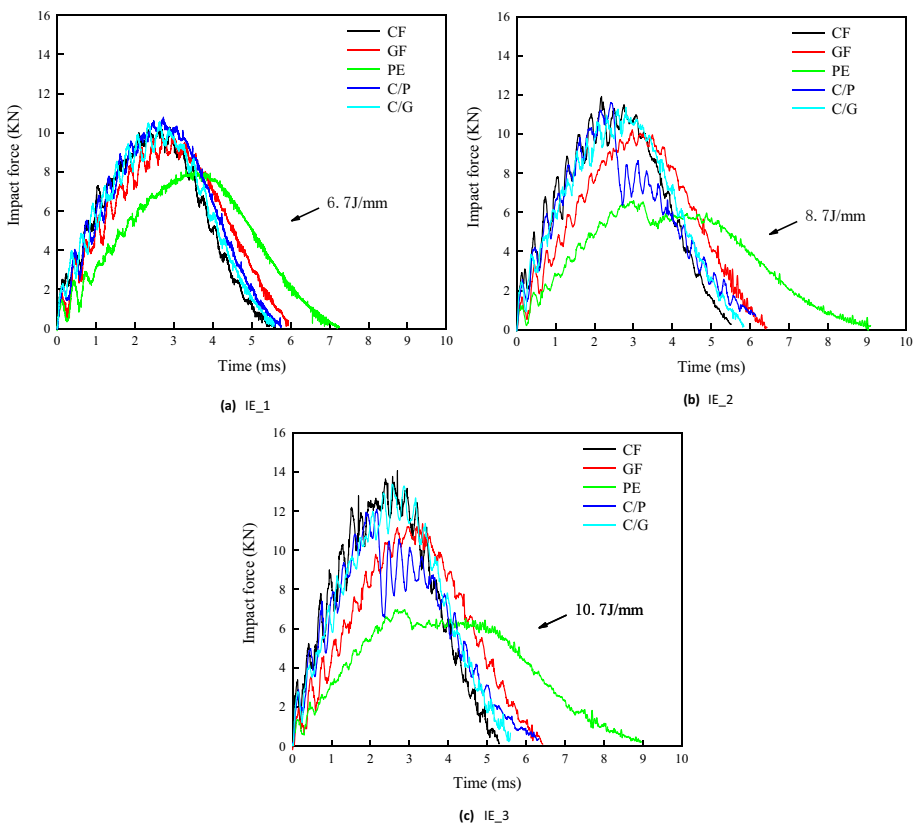


Fig. 3 Force–time responses of all the laminates for all the impact energies

properties of damaged polymer matrix composite plates” [29]. A 100 kN universal testing machine was used for this test. Using the support of the CAI fixture, the impacted specimens were loaded with a 1.2 mm/min displacement control crosshead to reduce loading eccentricity and any induced bending. During the test, the load curve and change in the moving distance with time were measured using the load cell and inductive displacement sensor. When the specimen broke or reached the maximum force of the test tool (100 kN), tests were stopped automatically. Three specimens were tested for each impact load and sample structure, and all tests were conducted three times before averaging the results.

3 Experiments Results and Discussion

3.1 Impact Tests

The five types of laminate specimens were each tested for the three impact levels, and because of reliable repeatability of the responses, only one specimen of each laminate was selected for representation in the impact curve. Figures 3 and 4 present the force–time and force–deflection curves for all the laminates. It is seen from Fig. 3 that the contact force increases with slight fluctuations until the peak force. All curves are symmetrical during

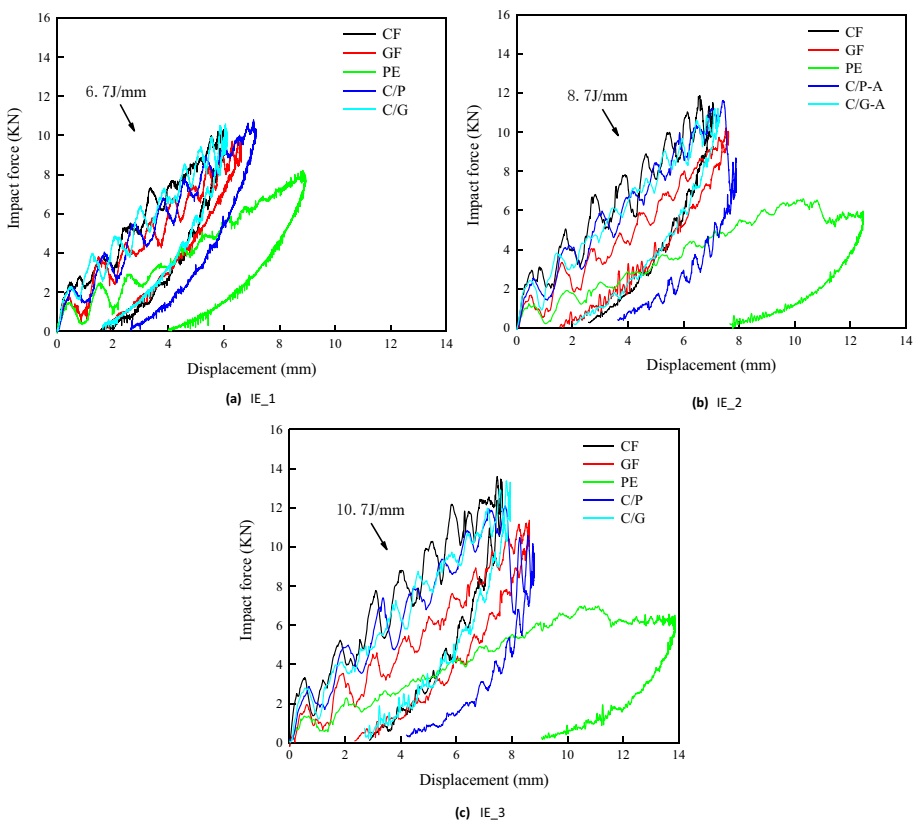


Fig. 4 Force–displacement responses of all the laminates for all the impact energies

loading and unloading and are similar to sinusoidal curves. As a general remark, the longer duration of impact contact force indicated more serious damage (especially fiber damage) inside layers. The oscillation of the force–time curve is mainly attributed to two reasons, namely the natural frequency caused by the infirm connection of the impactor component and bending vibrations of the impacted samples [30]. The first sudden drop in contact force was observed at the initial point of about 2 kN owing to matrix cracking or delamination of the composite laminate [31]. In Fig. 4, the resistance of the composite material to the impact load causes a rising part of the load–deflection curve, which is called the bending stiffness. When the impact increases, both the area of the closed curve and deflection increase.

Among the three impact levels, the slopes of the CF and C/G laminates were the highest, and the PE laminate displayed the largest response time (Fig. 3) and impact displacement (Fig. 4). With the increase in impact load, the PE and C/P laminates lose their load-carrying capacities and exhibit sudden drops in force after the peak force, indicating major damage initiation while the other three laminates do not show significant changes [32]. It is worth noting that after failure of the PE fiber laminates, the peak load showed relatively stable progressive failure with small fluctuations caused by the gradual expansion of the damaged area after initial fiber breakage along the fiber direction [33]. It is seen that the C/P curves fluctuate violently near the peak force and that the force values drop suddenly, which is associated with the failure of the PE fibers.

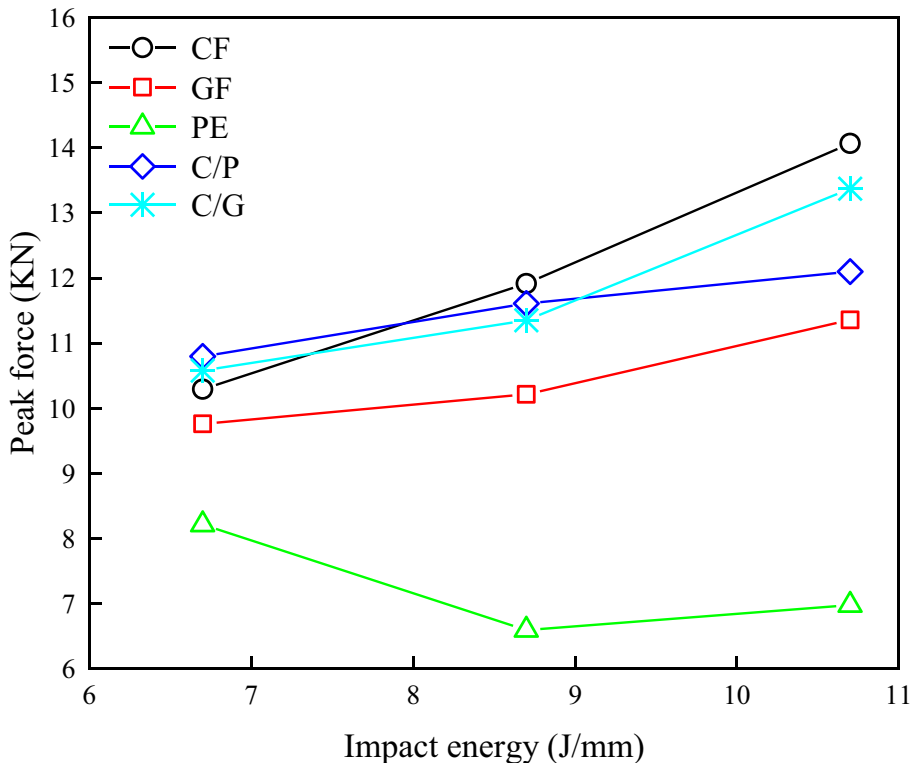


Fig. 5 Peak force values of all the laminates for all the impact energies

In addition, as evidenced by the experimental results, the C/G laminate exhibits higher impact loads, shorter impact times, and smaller impact displacements than the C/P laminate. Moreover, there are no-load drops for the C/G laminate, indicating that glass fibers have higher impact resistances than PE fibers. Given these observations, it is important to remember that the responses of laminates are not the same for different hybrid-fiber designs with significant variations.

Figure 5 indicates the maximum load that the composite laminate can withstand before it suffers major damage from an impact. As described in [15], the peak load increases with impact level, and the peak load of the C/P laminate is obviously better than that of the PE laminate, approaching the peak load of the CF laminate. Among these, when the impact level is 8.7 J/mm, only the peak load of the PE laminate decreases by 19.7%, and it can be inferred that the decrease in peak force at this time is due to fiber damage and fracture in the laminate layer. Similarly, the peak load of the C/G laminate is higher than that of the GF laminate and close to that of the CF laminate. It is therefore judged that the hybrid laminate inherits the characteristics of carbon fibers, resulting in positive hybrid synergistic effects and improved impact resistance.

Figure 6 shows the energy-time-history curves of the five types of laminates under the three impact levels. These impact levels can be divided into two parts, namely

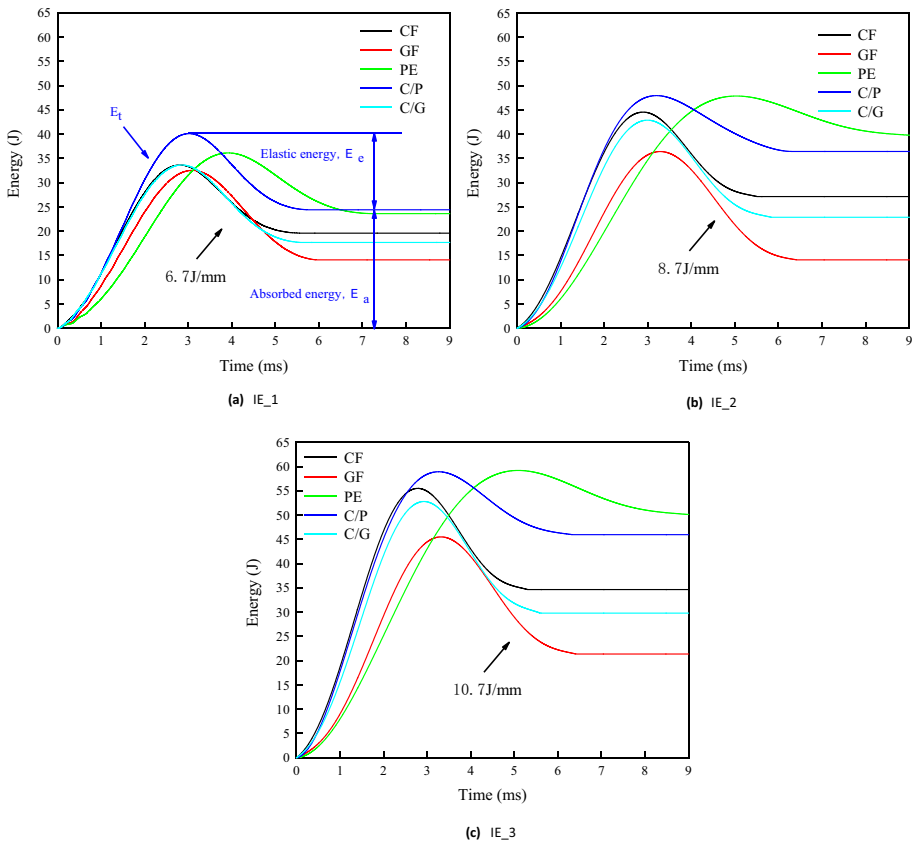


Fig. 6 Impact energy evolution of all the laminates for all the impact energies ()

elastic energy (E_e that is non-dissipated during the impact) and absorption energy (E_a that is dissipated during the impact), as shown for the C/P laminate in Fig. 6(a). And E_i is the maximum energy at maximum force. The relationship among E_i , E_e and E_a can then be written as follows [34]:

$$E_i = E_a + E_e \tag{1}$$

This absorbed energy (E_a) can be used as a damage index: the higher the absorbed energy, the higher is the damage, among which delamination, fiber breakage, and fiber shear are the main mechanisms of energy absorption [35–37]. Here, $E_a(t)$ is the energy absorbed by the composite at any time “ t ”, which can be calculated using Eq. (2), wherein “ $V(t)$ ”, “ V_i ”, “ m ”, “ g ”, and “ δ ” are the velocity of the impactor at time “ t ”, initial velocity, impactor mass, gravitational acceleration, and deflection [28]. In addition, the value of the absorbed energy can be obtained by calculating the area enclosed by the load–displacement curve [7, 38–40]. Table 4 can intuitively observe the absorbed energy of all laminates under each impact energy. Comparing the absorbed energy value calculated by Eq. (2) with the absorbed energy value obtained from the experiment, it can be found that the error between the two is extremely small, both within 1%.

$$E_a(t) = \frac{m(V_i^2 - V^2(t))}{2} + mg\delta(t) \tag{2}$$

The absorbed energy of each laminate was calculated using the time-energy curve plotted in Figs. 7(a) and (b). The magnitude and percentage of absorbed energy increase with increasing impact levels for all laminates. Moreover, the absorbed energies of all specimens show the same trends under each impact level. And the percentage of absorbed energy for different impact energies can be calculated as follows:

Table 4 Absorbed energy of laminates

Laminate	Normalized impact load (J/mm)	Impact velocity V_i, V_t (m/s)	Absorbed energy theoretical value (J)	Absorbed energy experimental value (J)	The error between the theoretical value and the experimental value (%)
CF	6.7	3.48, 2.24	19.51	19.59	0.43
	8.7	4.01, 2.50	27.03	27.15	0.43
	10.7	4.48, 2.74	34.55	34.65	0.30
GF	6.7	3.42, 2.57	14.00	14.09	0.63
	8.7	3.62, 2.55	18.16	18.09	0.30
	10.7	4.05, 2.94	21.34	21.36	0.11
PE	6.7	3.60, 2.11	23.40	23.61	0.91
	8.7	4.14, 1.69	39.28	39.74	1.17
	10.7	4.61, 1.79	49.63	50.14	1.02
C/P	6.7	3.80, 2.37	24.26	24.40	0.56
	8.7	4.16, 2.02	36.37	36.44	0.19
	10.7	4.61, 2.15	45.73	45.97	0.52
C/G	6.7	3.48, 2.39	17.60	17.68	0.48
	8.7	3.93, 2.68	22.72	22.88	0.70
	10.7	4.36, 2.87	29.62	29.80	0.59

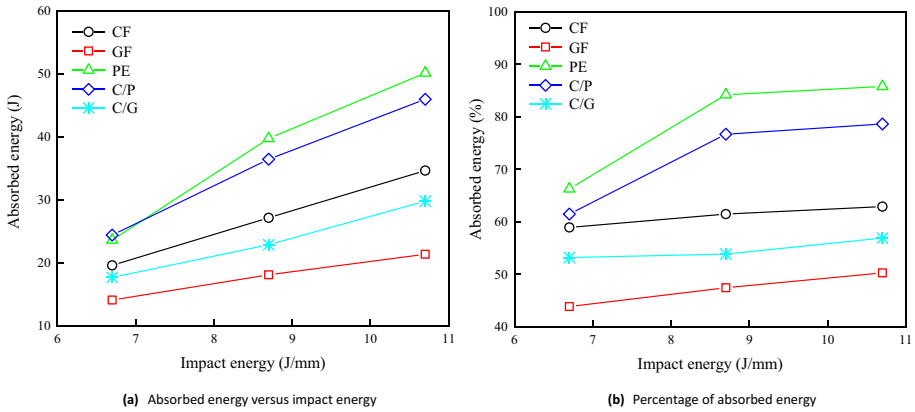


Fig. 7 Absorbed energy and percentage of absorbed energy for different impact energies

$$\eta = \frac{E_a}{E_i} \times 100\% \quad (3)$$

Of all the laminates, the percentage of absorption energy of PE is the highest (85.5%) while that of GF is the lowest (50.26%) at 10.7 J/mm. Further, the percentage of energy absorption of C/P laminate was significantly higher than that of C/G laminate by about 20%. It is seen that the energy consumption of the C/G laminate is lower than that of the C/P laminate, and the difference in absorbed energy between the C/G and C/P laminates increase with increasing impact levels, i.e., the damage in the C/P layer is more serious than that in the C/G layer. According to the research of A.R. et al. [41], this is because PE fibers are more flexible and have higher energy absorption capacities while glass fibers are hard and fragile with lower energy absorption capacities.

3.2 Impact Damage

Ultrasonic images were used to determine the damage extension (delamination) after low-velocity impact. Figure 8 illustrates the projected impact damage profiles of all laminates based on all impact levels from C-scan inspections. The color pattern of the C-scans indicates that the A-scan waveforms are a percentage of the screen height. The deeper the colors, the lower are the proportions of the waveforms, indicating higher degrees of damage to the laminate. It is worth noting that the A-scan is a point scan and a waveform; the B-scan is a line scan, which is a two-dimensional image; C-scan is a surface scan or projection scan, which is a two-dimensional image. Multiple A-scans constitute B-scans, and B-scans form C-scans. The ultrasonic study of PE and C/P laminates does not produce satisfactory results, which is attributed to the low refractive index of the PE fibers. All specimens show enhanced damage propagation with increasing impact levels, i.e., the lengths of the specimens along the X and Y directions increase gradually. Compared with the results of other laminates, there is a significant difference in the projected damage profile of the GF. When the impact level is 6.7 J/mm, the GF laminate exhibits a close-to-circular projected delamination profile, as observed in [42, 43], while other types of laminated areas have similar shapes and show cross-shaped layered profiles. With the increase in impact level, the projection damage profile of the GF changes gradually from circular to cruciform shape.

To evaluate the damage state caused by impact, two parameters are considered here, namely dent depth and damaged area [44]. Figure 9(a) and (b) present the evolution of the dent depths and projected damage areas of all specimens for 6.7, 8.7, and 10.7 J/mm impact levels. And the experimental data can also be observed intuitively through Table 5. In general, laminate deformation is generated when the materials are subjected to a certain load. Impact damage is normally detected through permanent impact dent depths of the impacted surfaces. The dent depths increased almost linearly with impact levels for all specimens (Fig. 9(a)). At the impact level of 6.7 J / mm, all samples except PE showed approximately the same dent depth, which was caused by the large plastic deformation of PE fiber. For higher impact levels, CF, GF, and C/G differed from PE and C/P, obviously showing lower dent depths. However, the indentation depth of C/P was significantly shallower than that of PE laminates. This phenomenon was attributed to the interlayer hybrid

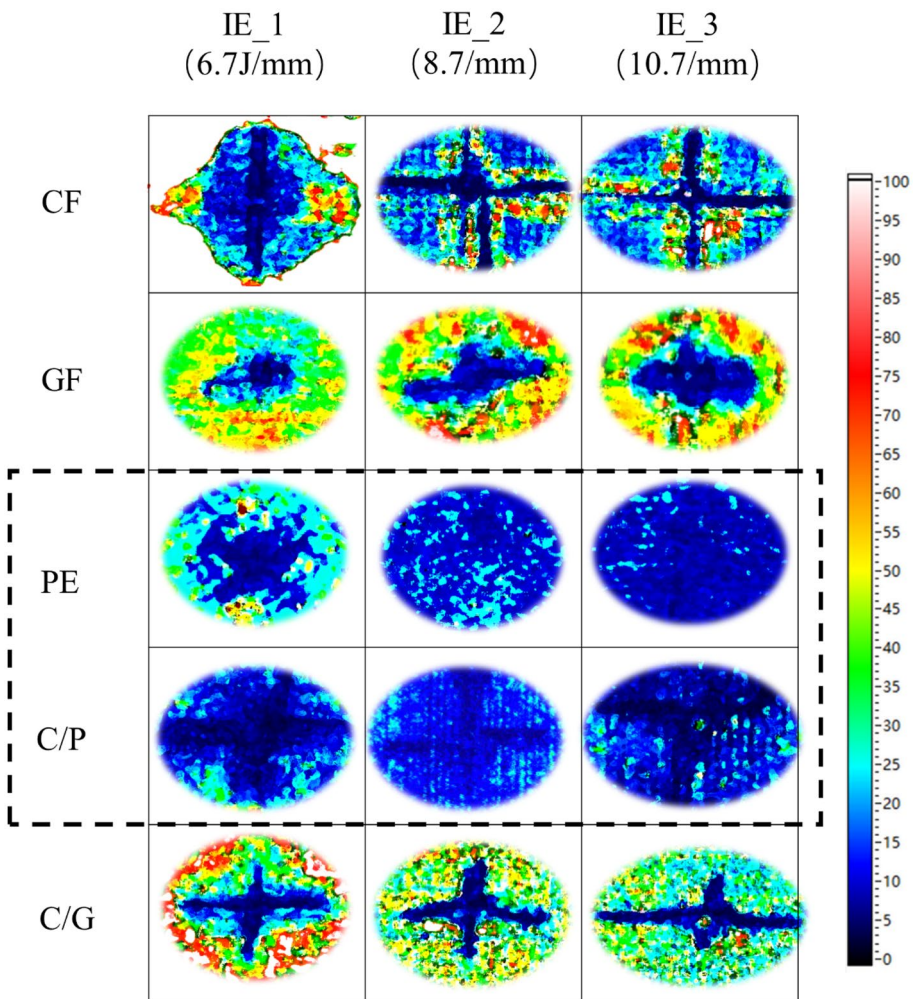
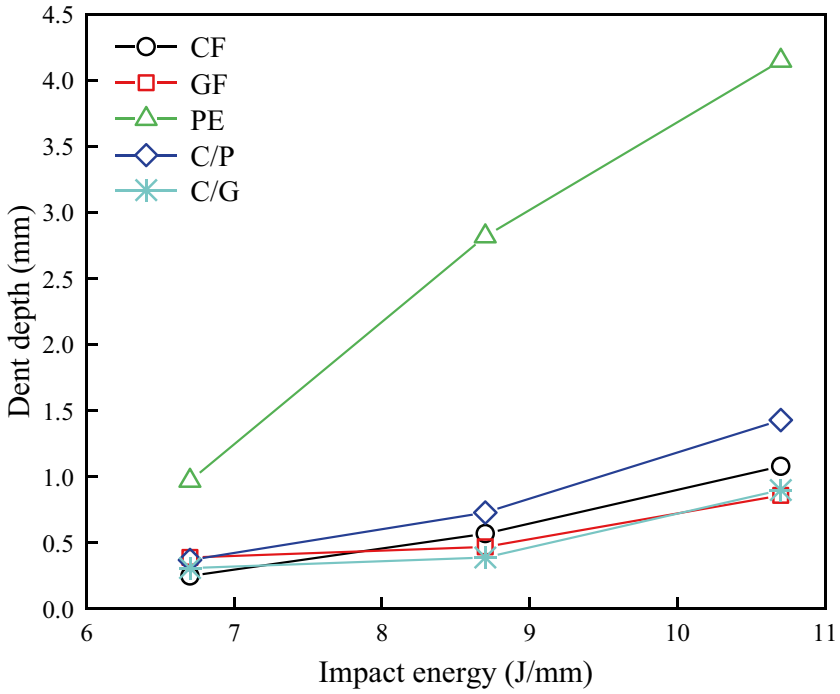
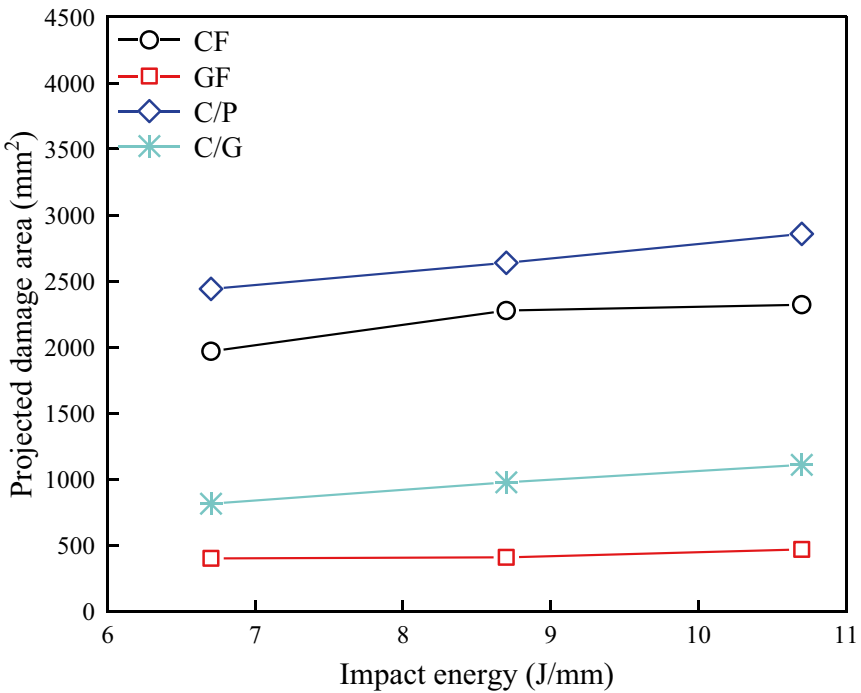


Fig. 8 Projected damage contours and areas obtained from the C-scan damage assessment of all laminates for all impact energies



(a) Dent depth values



(b) Damage area values

◀ Fig. 9 Values of the projected dent depth and damage area

structure which enhanced the interlayer bonding strength and toughness. Moreover, compared with C/G, the significant increase in C/P dent depth also supported the escalation of fiber breakage in C/P at higher impact levels.

According to Fig. 9(b), since the projected damage area is obtained by the ultrasonic C-scan, the area of PE laminate cannot be accurately obtained. The projected damage area of GF was between 400 mm² and 470 mm² and was always the smallest. And the projected damage area of C/P was the largest, which increased with the increase of impact energy, ranging from 2441 mm² to 2857.6 mm². It is noticeable that linear behavior can be identified for the laminates from Fig. 9(b), and the projected damage area of all specimens showed a nearly constant increase, where the projected damage area of C/P was approximately three times that of C/G. The increase in damaged area can be attributed to the increment in interlaminar stresses (shear stresses caused by bending), which leads to more serious interlayer damage in the form of delamination.

3.3 Post-impact Properties: CAI

3.3.1 Influence on Residual Strength

The residual strength evaluation of damaged specimens is a critical issue in the application of composite materials, and CAI is a common method for assessing the residual strength of

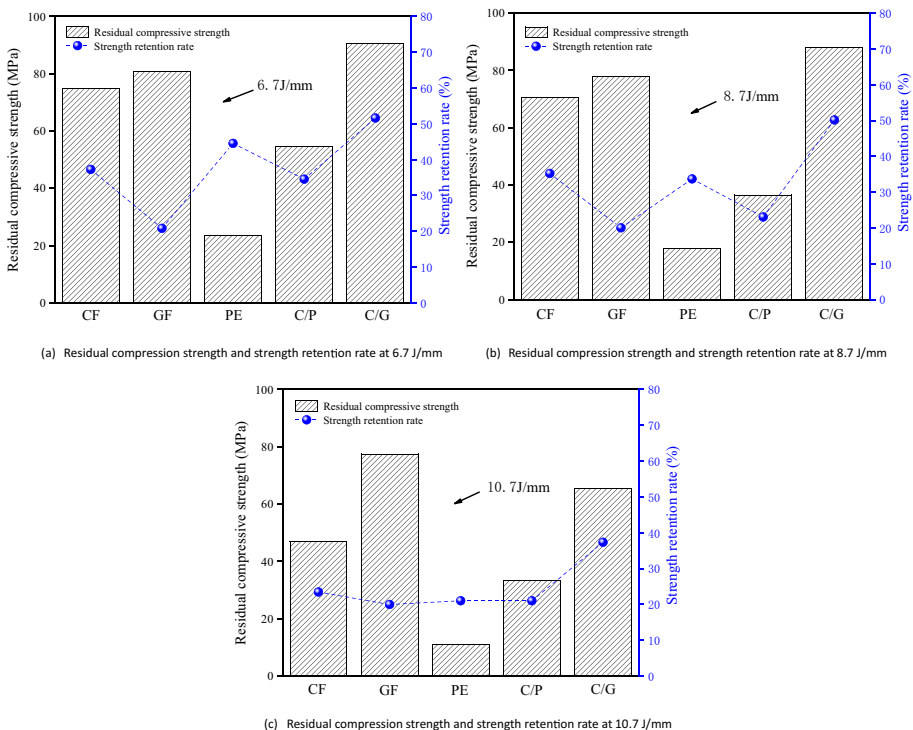


Fig. 10 Residual compression strength and strength retention rate for all impact energies

CFRP laminates. To investigate the post-impact material potential of seven different composites, compression after impact tests were performed.

Figure 10 presents both residual compression strength and strength retention rate values for all laminates. Table 5 also gives detailed information on the residual compression strength and strength retention rate of the five laminates under three different energies. The analysis of post-impact material potential showed that the compressive residual strength and strength retention rate values of the impacted specimens declined with the increase in the impact energy. It can also be noticed that for all impact cases, the CAI strength decreased with the increase in impact energy, which is due to delamination, fiber splitting and, matrix cracking [45]. Compared with carbon fiber and glass fiber, PE fiber had significant non-linear elasticity, which led to larger inelastic strain dissipated energy. Therefore, PE laminates possessed larger energy absorption under the same impact energy, resulting in more serious impact damage to the laminates, and then exhibited lower impact resistance and residual compressive strength. It can be found that when the impact energy was 6.7 J/mm, PE exhibited the smallest residual compressive strength. In addition, the strength retention rate of C/G was the highest under each impact energy, which was 20% higher than the strength retention rate of C/P on average. In particular, when the impact energy was 10.7 J/mm, the strength retention rate of C/G composite materials was about 40%, while the strength retention rate of C/P was the same as that of single-type laminate, with only 20%. This result means that the hybrid laminate composed of carbon fiber and glass fiber has more advantages in impact resistance and damage tolerance.

3.3.2 Failure Analysis

The front and side failure modes of different fiber-reinforced composites subjected to CAI are illustrated in Fig. 11. And Fig. 11(a) presents that after the CAI test, the surface of the

Table 5 Impact damage and post-impact properties

Laminate	Normalized impact load (J/mm)	Dent depth (mm)	Projected damaged area (mm ²)	Residual compressive strength (MPa)	Strength retention rate (%)
CF	6.7	0.25	1968.33	74.67	37.24
	8.7	0.57	2277.3	70.60	35.21
	10.7	1.08	2320.8	46.98	23.43
GF	6.7	0.39	401.67	80.67	20.79
	8.7	0.47	408.8	77.80	20.05
	10.7	0.86	468.9	77.46	19.96
PE	6.7	0.97	—	23.33	44.51
	8.7	2.82	—	17.67	33.71
	10.7	4.15	—	11	20.98
C/P	6.7	0.37	2441	54.5	34.51
	8.7	0.73	2638.8	36.44	23.08
	10.7	1.43	2857.6	33.16	21.00
C/G	6.7	0.31	815	90.57	51.60
	8.7	0.39	976.6	88.03	50.16
	10.7	0.9	1109.3	65.48	37.13

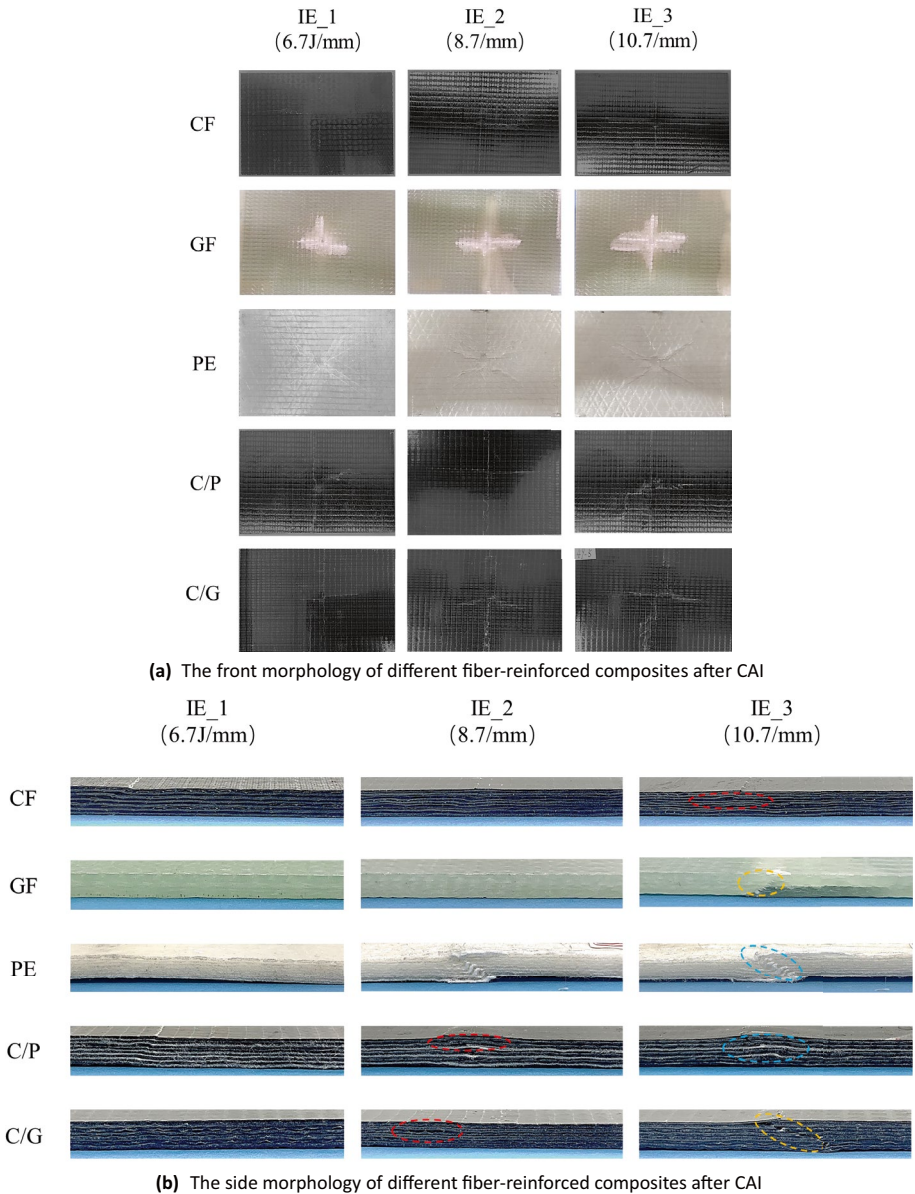


Fig. 11 The morphology of different fiber-reinforced composites after CAI

PE laminate has obvious wrinkles, while the surface of the remaining laminates due to the damage induced by bending, showing macro-cracks aligned along the longitudinal yarn direction. The location of the dominant fracture surface of all CAI specimens is similar and constant, close to the central cross-section, and propagated throughout the specimen. The dominant damage modes of CF, GF, and PE were delamination, cracking, and wrinkling in Fig. 11(b), respectively, which were indicated by red, yellow, and blue dotted lines. And

the extent of the damage to each laminate gradually increased with the increasing impact of energy. It can be found from the side failure modes of different fiber-reinforced composites that the hybrid fiber laminate inherited the failure mode of the single laminate and the delamination occurred in the direction perpendicular to the load direction. The damage modes of *C/P* were a combination of delamination damage and wrinkling of the fiber layer, while the failure mode of *C/G* was delamination damage and interlaminar fracture. It can be found that delamination is initiated in the direction perpendicular to the load direction and propagated in different directions as a function of the fiber orientation [46]. Furthermore, it can be seen from the CAI test specimen that the side damage of the specimen just occurred at the vertical position of the impact point, that is, the center position of the side length of the specimen. This is because fiber fractures near the front surface due to compression during impact, resulting in stress redistribution and stress concentration under subsequent CAI.

The microscopic observation of the impact point after CAI is illustrated in Fig. 12. Since we cannot clearly observe the damage state at the impact point on the surface of the laminate after the CAI test with the naked eyes in Fig. 11(a), we have carried out optical microscopic tests to better observe the microscopic damage morphology at the impact point after CAI. And some differences could be observed by analyzing the impact point

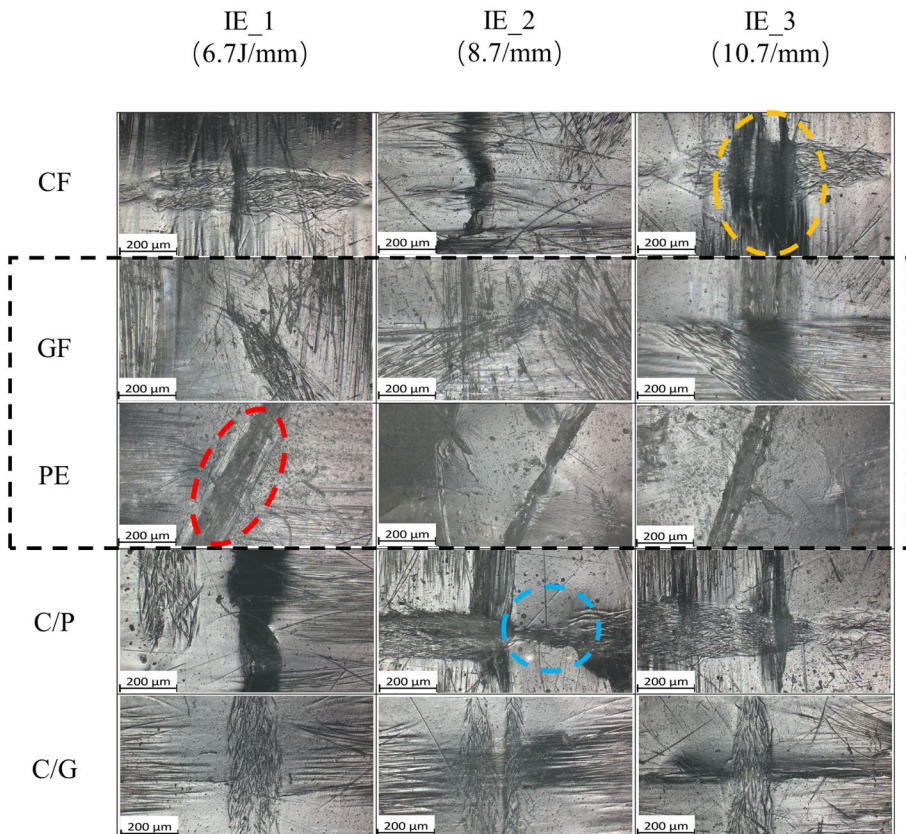


Fig. 12 Microscopic observations of different fiber-reinforced composites at impact positions after CAI

micrograph. Matrix cracks and fiber breakage were marked yellow and blue, respectively, and the red dashed line represented the thin lines of the strapping layer of cloth. According to Fig. 12, CF, C/P, and C/G displayed a cruciform failure state, and the fiber and matrix of CF were damaged most seriously at an impact energy of 6.7 J/mm. Obviously, the occurrence and severity of damage increased with the increase of the impact energy. Due to the characteristics of the material itself, there is no obvious damage to the surface impact points of GF and PE. It can be seen that the matrix damage caused by low-velocity impact initiated from the central impacted zone and propagates to the two free edges. The local damage of the matrix caused the fibers near the damaged area of the matrix to lose the support of the matrix, and then the local buckling and delamination damage occurred.

4 Conclusion

LVI impact tests with different impact energies and compression after impact tests were performed to identify the influence of different fiber compositions within laminates and evaluate the damage resistance and tolerance of each laminate for the selection of marine laminated materials. From the evaluation of the experimental results, the following conclusions can be drawn:

- Hybrid laminates inherited the material properties of the single-type laminates and had a positive impact on LVI impact due to the inter-fiber hybrid effect. C/G improved the toughness due to fiber mixing, while C/P exhibited higher energy absorption due to the enhanced ductility of fiber hybrids.
- GF laminates exhibited a close-to-circular projected delamination profile, while other types of laminated areas presented a cross-shaped layered profile. Due to the larger plastic deformation of PE fiber, PE and C/P obviously showed deeper dent depth. And the projected damage area of all specimens showed a nearly constant level increase, where the projected damage area of C/P was approximately three times that of C/G.
- In addition, the hybrid laminates had a stronger strength retention rate, which was about 40% higher than the single-type laminates in the highest impact case. Among them, C/G exhibited better impact damage resistance and stronger impact damage tolerance than C/P. This was demonstrated through CAI tests, especially when the impact energy was 10.7 J/mm, the residual compressive strength of C/G was about twice that of C/P, and the strength of retention was about three times that of C/P.
- The main failure modes of laminates subjected to CAI were delamination, cracking, and wrinkling, respectively. Through microscopic observation, it is seen that the fiber and matrix of CF were the most damaged. With the increase of impact energy, the occurrence and severity of damage of all materials have also increased.

Data Availability The raw/processed data required to reproduce these findings cannot be shared at this time as the data also forms part of an ongoing study.

Declarations

Conflict of Interest The authors declare no competing financial interest.

References

1. Sutherland, L.S.: A review of impact testing on marine composite materials: Part I - Marine impacts on marine composites. *Compos. Struct.* **188**, 197–208 (2018)
2. Sutherland, L.S.: A review of impact testing on marine composite materials: Part II – Impact event and material parameters. *Compos. Struct.* **188**, 503–511 (2018)
3. Rivallant, S., et al.: Experimental analysis of CFRP laminates subjected to compression after impact: The role of impact-induced cracks in failure. *Compos. Struct.* **111**, 147–157 (2014)
4. Rhead, A.T., Hua, S., Butler, R.: Damage resistance and damage tolerance of hybrid carbon-glass laminates. *Compos. A Appl. Sci. Manuf.* **76**, 224–232 (2015)
5. Koo, J.M., Choi, J.H., Seok, C.S.: Prediction of post-impact residual strength and fatigue characteristics after impact of CFRP composite structures - Science Direct. *Compos. B Eng.* **61**(5), 300–306 (2014)
6. Liu, B., et al.: Study on impact damage mechanisms and TAI capacity for the composite scarf repair of the primary load-bearing level. *Compos. Struct.* **181**, 183–193 (2017)
7. Tuo, H., et al.: Damage and failure mechanism of thin composite laminates under low-velocity impact and compression-after-impact loading conditions. *Compos. B Eng.* **163**, 642–654 (2019)
8. Tan, et al. Predicting low velocity impact damage and Compression-After-Impact (CAI) behaviour of composite laminates. *Compos. Part A Appl. Sci. Manufact.* **71A**, 212226 (2015)
9. Li, X., et al.: Assessment of failure criteria and damage evolution methods for composite laminates under low-velocity impact. *Compos. Struct.* **207**, 727–739 (2019)
10. Meola, C., et al.: Nondestructive evaluation of carbon fibre reinforced composites with infrared thermography and ultrasonics. *Compos. Struct.* **134**, 845–853 (2015)
11. Sevkat, E., Liaw, B., Delale, F.: Drop-weight impact response of hybrid composites impacted by impactor of various geometries. *Mater. Design* **52**, 67–77 (2013)
12. Swolfs, Y., et al.: The importance of translaminar fracture toughness for the penetration impact behaviour of woven carbon/glass hybrid composites. *Compos. A Appl. Sci. Manuf.* **103**, 1–8 (2017)
13. Bulut, M., Erklig, A.: The investigation of quasi-static indentation effect on laminated hybrid composite plates. *Mechanics of Maters.* **117**, 225–234 (2017)
14. Chen, D., et al.: Low velocity impact behavior of interlayer hybrid composite laminates with carbon/glass/basalt fibres. *Compos. Part B: Eng.* **176**, 107191 (2019)
15. Zhang, C., Rao, Y., Li, W.: Low-velocity impact behavior of intralayer hybrid composites based on carbon and glass non-crimp fabric. *Compos. Struct.* **234**, 111713 (2020)
16. Cheon, J., Lee, M., Kim, M.: Study on the stab resistance mechanism and performance of the carbon, glass and aramid fiber reinforced polymer and hybrid composites. *Compos. Struct.* **234**, 111690 (2020)
17. Hung, P., et al.: Impact response of hybrid carbon/glass fibre reinforced polymer composites designed for engineering applications. *Compos. B Eng.* **133**, 86–90 (2018)
18. Liu, H., et al.: Experimental and numerical studies on the impact response of damage-tolerant hybrid unidirectional/woven carbon-fibre reinforced composite laminates. *Compos. Part B. Eng.* **136B**, 101–118 (2020)
19. Zhao, Z., et al.: Effect of fiber architecture on the impact resistance of composite panels subjected to metallic projectile. *Compos. Struct.* **273**, 114273 (2021)
20. Jakubczak, P., Bienia, J., Drodziel, M.: The collation of impact behaviour of titanium/carbon, aluminum/carbon and conventional carbon fibres laminates. *Thin-Walled Struct.* **155**(13), 106952 (2020)
21. Zhao, Z., et al.: On the impact failure behavior of triaxially braided composites subjected to metallic plate projectile. *Compos. Part B: Eng.* **186**, 107816 (2020)
22. Aktas, A., Aktas, M., Turan, F.: Impact and post impact (CAI) behavior of stitched woven-knit hybrid composites. *Compos. Struct.* **116**, 243–253 (2014)
23. Evci, C., Guelgec, M.: An experimental investigation on the impact response of composite materials. *Int. J. Impact Eng* **43**, 40–51 (2012)
24. Krollmann, J., et al.: Impact and post-impact properties of hybrid-matrix laminates based on carbon fiber-reinforced epoxy and elastomer subjected to low-velocity impacts. *Compos. Struct.* **208**, 535–545 (2019)
25. Sanchez-Saez, S., et al.: Compression after impact of thin composite laminates. *Compos. Sci. Technol.* **65**(13), 1911–1919 (2005)
26. Saeedifar, M., et al.: Damage assessment of NCF, 2D and 3D woven composites under compression after multiple-impact using acoustic emission. *Compos. Part A: Appl. Sci. Manufact.* **132**, 105833 (2020)
27. Sharma, K.K., et al.: Evaluation of flexural strength of hybrid FRP composites having three distinct laminates. *Materials Today: Proceedings* **38**, 418–422 (2021)

28. ASTM D7136/D7136–15.: Standard test method for measuring the damage resistance of a fiber reinforced polymer matrix composite to a drop weight impact event (2015)
29. ASTM D7137/D7137–12.: Standard Test Method for Compressive Residual Strength Properties of Damaged Polymer Matrix Composite Plates (2012)
30. Gliszczynski, A., et al.: The response of laminated composite plates and profiles under low-velocity impact load - ScienceDirect. *Compos. Struct.* **207**, 1–12 (2012)
31. Sarasini, F., et al.: Hybrid composites based on aramid and basalt woven fabrics: Impact damage modes and residual flexural properties. *Mater. Design* **49**, 290–302 (2013)
32. Sarasini, F., et al.: Effect of basalt fiber hybridization on the impact behavior under low impact velocity of glass/basalt woven fabric/epoxy resin composites. *Compos. A Appl. Sci. Manuf.* **47**, 109–123 (2013)
33. Xu, Z., et al.: An experimental and numerical study on scaling effects in the low velocity impact response of CFRP laminates. *Compos. Struct.* **154**, 69–78 (2016)
34. Ay, A., et al.: Revealing the effects of matrix behavior on low-velocity impact response of continuous fiber-reinforced thermoplastic laminates. *Compos. Struct.* **210**, 239–249 (2019)
35. Quaresimin, M., et al.: Energy absorption in composite laminates under impact loading. *Compos. B Eng.* **44**(1), 133–140 (2013)
36. Zhou, G.: Damage mechanisms in composite laminates impacted by a flat-ended impactor. *Compos. Sci. Technol.* **54**(3), 267–273 (1995)
37. Papa, I., et al.: Ultrasonic damage investigation on woven jute/poly (lactic acid) composites subjected to low velocity impact. *Compos. Part B Eng.* **115**, 282–288 (2017)
38. Ravandi, M., et al.: Low velocity impact performance of stitched flax/epoxy composite laminates. *Compos. B Eng.* **117**, 89–100 (2017)
39. Liao, B.B., Liu, P.F.: Finite element analysis of dynamic progressive failure properties of GLARE hybrid laminates under low-velocity impact. *J. Compos. Mater.* **52**(10), 1317–1330 (2018)
40. Zhou, J., et al.: Low-velocity impact behavior and residual tensile strength of CFRP laminates. *Compos. B Eng.* **161**, 300–313 (2019)
41. Conway, R.: Handbook of Technical Textiles || Technical textile finishing. 189–210 (2016)
42. González, E.V., et al.: Simulating drop-weight impact and compression after impact tests on composite laminates using conventional shell finite elements. *Int. J. Solids Struct.* 144–145 (2018)
43. Soto, A., et al.: Low velocity impact and compression after impact simulation of thin ply laminates. *Compos. Part A, Appl. sci manufact* **109**, 413–427 (2018)
44. Sun, X.C., Hallett, S.R.: Failure mechanisms and damage evolution of laminated composites under compression after impact (CAI): Experimental and numerical study. *Compos. A Appl. Sci. Manuf.* **104**, 41–59 (2018)
45. Selver, E., et al.: Impact damage tolerance of thermoset composites reinforced with hybrid commingled yarns. *Compos. Part B Eng.* **91**, 522–538 (2016)
46. Sebaey, T.A., et al.: Damage resistance and damage tolerance of dispersed CFRP laminates: Effect of the mismatch angle between plies. *Compos. Struct.* **101**(12), 255–264 (2013)

Publisher's Note Springer Nature remains neutral with regard to jurisdictional claims in published maps and institutional affiliations.